IEEE Access
Multidisciplinary | Rapid Review | Open Access Journal

Received September 11, 2019, accepted October 31, 2019, date of publication November 11, 2019,
date of current version November 21, 2019.

Digital Object Identifier 10.1109/ACCESS.2019.2952953

Research on Detection Method of Small Size Weld Bead Defects Based on Reluctance Measurement

HONGMIN WANG AND MENG WANG
Department of Automation, Harbin University of Science and Technology, Harbin 150080, China
Corresponding author: Hongmin Wang (13904810908@163.com)

This work was supported in part by the Heilongjiang Province Natural Science Foundation of China under Grant F201310.

ABSTRACT To achieve non-destructive testing for small size weld beads of metal workpieces, we developed a new testing method of closed magnetic circuit reluctance measurement. According to the shape and volume of the small size weld defects of the metal workpiece, a reluctance detection model was established in the detection environment of alternating magnetic field. The relationship between different weld defects and closed magnetic circuit reluctance was quantitatively analyzed to achieve the identification of weld defects. A particle swarm optimization algorithm (PSO) was applied to optimize the cost-sensitive support vector machine (CS-SVM), which effectively reduced the coupling errors caused by the limitation of the workpiece coupling size. This new method was used to verify the weld bead detection of representative carbide saw blades. Compared with the basic support vector machine, the improved cost-sensitive support vector machine has better performance in the classification of unbalanced samples. The experimental results showed this new method can detect the weld bead of carbide saw blade with the correct rate to 98.2%. It reduced the interference of coupling error effectively. The improved cost-sensitive support vector machine not only improved the detection accuracy, but also avoided the possibility that the defective weld workpiece samples are misclassified into qualified workpieces. This study provides a guarantee for safe production and has great significance in engineering applications. The new method provides an effective solution for the application of reluctance testing technology in small size weld bead detection.

INDEX TERMS Closed magnetic circuit, cost-sensitive support vector machine, coupling error, particle swarm optimization, reluctance measurement, small size weld bead.

I. INTRODUCTION

Due to the requirements of product safety, welding technology, as one of the most commonly used processing methods of industrial products, has received increasing attention. Currently, butt welding is one of the most widely used welding methods because of its low cost. However, this method is prone to low welding fastness and lack of fusion when the metal material is affected by high temperature, which seriously affects the quality of workpiece. If the unqualified workpieces are used in industrial production, it does not cause equipment damage, but also introduces safety hazards. Therefore, it is critical to detect the welding quality of the workpiece. Non-destructive testing has become one of the most popular testing methods in engineering due to its non-destructive, dynamic and strict advantages [1]. However, there are a number of limitations in the state-of-the-art non-destructive testing methods for the detection of small size weld bead.

In the non-destructive testing of metal workpieces, although the resolution of radiographic testing is high, its management, usage and maintenance are limited because of the radioactive radiation. Penetrant testing can only detect surface defects, which is complicated and inefficient. Ultrasonic testing needs to fill the gap between the probe and the measured surface with couplant. For thinner objects, the accuracy of ultrasonic testing is reduced or even missed. The magnetic particle testing has the highest defect resolution, but it has higher requirements than other detection techniques, such as smooth surfaces, etc [2]–[4]. Therefore, the above testing methods are not suitable for the production line detection of workpieces with large production capacity, a large number of welding processes and a small weld size.

In order to improve the detection ability, intensive research has been carried out in the field of non-destructive testing. For example, Rodríguez-Gonzálvez and

The associate editor coordinating the review of this manuscript and approving it for publication was Jenny Mahoney.

Rodríguez-Martín [5] focused on the study of 3D features on real cases to identify the most relevant ones for weld bead detection on the basis of the information gain. By analyzing the influence of neighborhood size for covariance matrix computation, decision tree algorithms, and split criteria, optimization results are obtained. Gurieva *et al.* [6] carried out experiments and compared the non-destructive testing effects of visual testing, penetrant testing, ultrasonic testing, radiographic testing and other methods on PF1 coil welds. NDT is capable to detect both surface imperfections and internal flaws, both volumetric and plane defects of all types of PF1 welds. Wu *et al.* [7] proposed a new non-destructive testing method for macroscopic defects of materials based on the variation of differential permeability in the biased magnetization field. It not only improved defect-recognition but also facilitated defect depth recognition. Carrigan *et al.* [8] proposed a new non-destructive testing method based on microwave and millimeter-wave reflection methods and improved non-destructive testing of nonmetallic pipes. Brizuela *et al.* [9] improved the image quality obtained by the phased array ultrasonic technique by combining three ultrasonic techniques, including Phased Array with dynamic depth focusing in reception, Synthetic Aperture Focusing Technique (SAFT) and Phase Coherence Imaging (PCI). The above studies have suggested new methods or improved related algorithms for non-destructive detection of large size samples, but the detection of small size weld bead still needs further study.

In order to resolve the problem that small size weld bead detection method is not enough to realize on-line detection, we proposed a new non-destructive testing method based on reluctance measurement and the improved cost-sensitive support vector machine model, which combined the stability and accuracy of reluctance attributes in a closed magnetic circuit. In this method, we placed the small weld metal workpiece in a closed magnetic circuit, and the closed magnetic field is formed by the core winding excitation coils. Magnetic cores are closely connected with magnetic yokes. Magnetic yokes contacted workpieces and ensured that the magnetic flux passed through the weld bead. According to the information of reluctance and other physical attributes in closed magnetic circuit, we can explore the defect type of workpiece weld bead. Because of its high sensitivity, this method is especially suitable for the detection of small size weld bead in metal workpieces. But it requires high coupling degree of reluctance in the measurement circuit. Even millimeter-scale coupling airgaps will lead to abnormal change of total reluctance, which seriously affects the accuracy of test results [10]. Therefore, the improved cost-sensitive support vector machine is trained by collecting relevant feature data, and the kernel width and misclassification cost parameters are optimized by particle swarm optimization algorithm. It has the ability to distinguish weld defects from coupling airgaps and to reduce coupling errors. The improved cost-sensitive support vector machine is used to assist the reluctance measurement method to realize the accurate detection of small size weld bead in closed magnetic circuits.

This method was applied to conduct a confirmatory experiment on a weld of a representative carbide saw blade. The material of carbide saw blade is mainly tungsten steel alloy. Its base thickness is 1.5 mm and the cutter teeth thickness is 3 mm. The welding defects of carbide saw blades mainly include cracks, pores, lack of fusion and cavities. Experiments were carried out to verify the reliability of the non-destructive method based on reluctance measurement. The classification performance of the improved support vector machine and the basic support vector machine was compared with different proportion of unbalanced samples.

This paper contains six parts. In the first part, we introduce the theme, the background of the topic and the workflow of the new method. In the second part, we discuss the advantages of using a closed magnetic circuit. Then we proposed the testing model of reluctance and the application of the detection system. In the third part, the particle swarm optimization algorithm was applied to improve the cost-sensitive support vector machine and use the collected feature data to train the improved cost-sensitive support vector machine. In the fourth part, the finite element simulation model was established. The types and models of defects are fully designed by software to determine the excitation signals and relevant adaptive parameters. In the fifth part, we verify the effects of weld defect types on inductance and reluctance under ideal conditions respectively. Then we carry out the experiments to obtain the test results in the actual physical environment. The classification results of the improved cost-sensitive support vector machine and the basic support vector machine for class imbalance samples are compared to verify the correctness of the method used in this paper. In the sixth part, we summarize the new methods and expound the advantages of the new methods.

II. MODEL CONSTRUCTION AND APPLICATION

A. MODEL CONSTRUCTION

For establish the detection environment, this paper first compares the amplitude of the magnetic flux density of the measured object in three different environments. All three detection environments consist of excitation coils with the same number of turns, and a 20 mA AC excitation signal was applied to each coil. In the first group of experiments, only an excitation coil was used to magnetize the measured workpiece, which constituted an open-circuit detection system. In the second group, excitation coils were wound on the magnetic core to magnetize the measured workpiece, which also constituted an open-circuit detection system. In the third group, excitation coils were wound on the core. Magnetic yokes ware used to connect cores and workpieces to form a closed magnetic circuit detection system. The finite element simulation of three groups experiment is shown in Fig. 1.

In Fig. 1, the arrow direction indicates the direction of magnetic flux flow, and the color represents the amplitude of magnetic flux density. The numerical model shown in Fig. 1 (a)

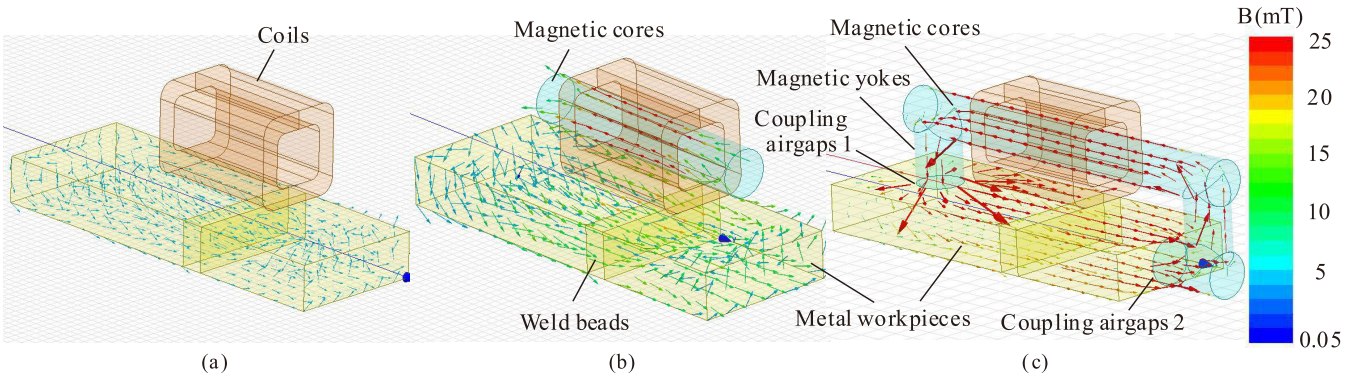

FIGURE 1. Comparison of magnetic flux density under three detection environments. (a) Only coils magnetize a workpiece. (b) Coils wound around the surface of the core magnetizes a workpiece. (c) Magnetic cores winding coils and magnetic yokes form a closed magnetic circuit to magnetize a workpiece.

is characterized by smaller magnetic flux density, and less magnetic flux flowing through the measured workpiece. The numerical model shown in Fig. 1 (b) is characterized by high magnetic flux density and more magnetic flux flowing through the measured workpiece. The numerical model shown in Fig. 1 (c) is characterized by the strongest magnetic flux density, which shows the design of a closed magnetic circuit effectively increasing the flux flowing in the workpiece. At the same power consumption, a closed magnetic circuit can greatly reduce magnetic leakage to ensure the maximum magnetic flux density. At the same time, considering the requirement of air medium for detection of small size weld defects, closed magnetic circuit provides guarantee for the accuracy of detection.

In summary, the non-destructive testing method of reluctance measurement is based on the physical environment of a closed magnetic circuit. The path of magnetic flux always concentrates and passes through a medium with low reluctance [11]. As shown in Fig. 1 (c), the non-destructive testing model for reluctance measurement consists of magnetic yokes, magnetic cores, excitation coils, metal workpieces, weld beads and coupling airgaps. By passing an AC excitation signal into excitation coils, and alternating magnetic field is generated around coils, which is used as the testing environment for reluctance measurement. According to the theory of reluctance, the magnetic flux must enter the workpiece through magnetic yokes. The two ends of magnetic yokes are in contact with the workpiece. One end is close to the measured weld beads and the other end is far from the weld beads. The designed structure ensures that the magnetic flux passes through the measured weld bead and is recycled by magnetic yokes.

If there are defects in the small size weld bead of the workpiece, the volume and quality of the weld material will change. The weld material is no longer compact and regular, and the weld bead is randomly filled with voids or pores of various shapes. The change of internal structure leads to the change of physical properties and then affects the change of physical quantities such as reluctance and magnetic flux.

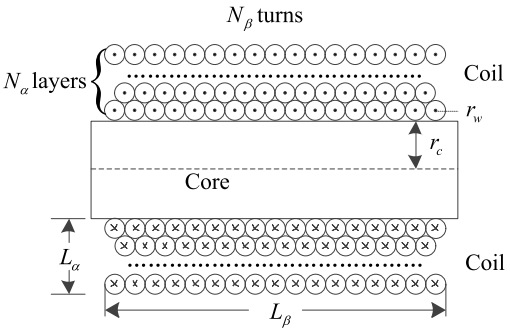

FIGURE 2. Expansion structure of excitation coils and magnetic cores.

In the process of small size weld defect detection, the contact between magnetic yokes and workpieces can not reach the micron level standard, and reasonable coupling airgaps will be generated in the coupling process. Usually, the coupling airgap and weld defect are small in size. It is approximated that the magnetic circuit is filled with the uniform magnetic field and the iron loss is neglected [12]. Because the alternating magnetic field is unsaturated, the magnetic flux density is not affected by the edge effect. In order to obtain the relevant parameters of the detection system, the internal structure of excitation coils and magnetic cores are unfolded, as shown in Fig. 2.

We divide the magnetic circuit into six parts in series. The total reluctance is the sum of the reluctance of each part as follows:

$$R_m = R_1 + R_2 + R_3 + R_4 + R_\gamma + R_{mw} \tag{1}$$

where R_1, R_2, R_3, and R_4 are the reluctance of magnetic yokes, the reluctance of coupling airgaps 1, the reluctance of coupling airgaps 2 and the reluctance of metal workpiece, respectively. Coupling airgaps 1 are gaps with air as the medium, which are generated between metal workpieces and magnetic yokes due to the loose coupling. And coupling airgaps 2 are generated between the other end of metal workpieces and magnetic yokes closing to weld beads. The R_γ and R_{mw} are the reluctance of measured weld bead and

the reluctance of magnetic core, respectively. Among them, the weld reluctance includes the reluctance $R_{\gamma 1}$ of the air medium at the weld defect and the reluctance $R_{\gamma 2}$ of the weld material at the defect. The reluctance of each part of the magnetic circuit is related to the length of each magnetic circuit, the cross-sectional area of each magnetic circuit and the permeability of the material. Then, R_m can be written as,

$$R_m = \frac{l_1}{\mu_0\mu_1 A_1} + \frac{l_2}{\mu_0 A_2} + \frac{l_3}{\mu_0 A_3} + \frac{l_4}{\mu_0\mu_4 A_4} + \frac{l_{\gamma 1}}{\mu_0 A_{\gamma 1}} + \frac{l_{\gamma 2}}{\mu_0\mu_{\gamma 2} A_{\gamma 2}} + R_{mw} \quad (2)$$

where l_1, l_2, l_3, and l_4 are the length of magnetic yokes, the length of coupling airgaps 1, the length of coupling airgaps 2 and the length of metal workpieces, respectively. A_1, A_2, A_3, and A_4 are the corresponding magnetic circuit cross-sectional areas. $l_{\gamma 1}$ and $l_{\gamma 2}$ are the length of weld defects and the length of weld material at defects, respectively. $A_{\gamma 1}$ and $A_{\gamma 2}$ are the corresponding magnetic circuit cross-sectional areas. μ_0 is vacuum permeability, which is equal to $4\pi \times 10^{-7}$H/m. μ_1, μ_4, and $\mu_{\gamma 2}$ are the relative permeability of magnetic yokes, the relative permeability of metal workpieces and the relative permeability of weld material at defects, respectively. The magnetic yoke material for oriented silicon steel, relative permeability of μ_1 approximately 7000-10000. Choosing oriented silicon steel not only effectively increases the binding magnetic ability of magnetic yokes, but also has the fairly small reluctance, which has little effect on the reluctance measurement [13].

In Fig. 2, the turn number N of the excitation coil wound on the magnetic core can be decomposed into the product of N_α and N_β, where N_α and N_β are the layer number of excitation coils winding and the number of turns wound by a single-layer excitation coil, respectively [14]:

$$N_\alpha = \frac{L_\alpha}{2r_w} \quad (3)$$

$$N_\beta = \frac{L_\beta}{2r_w} \quad (4)$$

where L_α, L_β, and r_w are the winding thickness of the excitation coil, the winding width of the excitation coil and the cross-section radius of the coil, respectively. The reluctance of the core in (1) can be written as,

$$R_{mw} = \frac{\sum_{i=1}^{N} I_i}{\phi} = \frac{NI}{\phi} = 4.44 \times N \times f \cdot \frac{N_\alpha \cdot N_\beta}{R_w} \quad (5)$$

where I, f, ϕ, and R_w are the excitation current, signal frequency, magnetic flux of core and the resistance of the excitation coil, respectively. Let l_w, A_w, and ρ denote the length of the coil, the cross-sectional area of the coil and the resistivity of the coil, respectively. According to the winding structure of the excitation coil in Fig. 2, the length and cross-sectional area of the excitation coil can be calculated as follows:

$$\begin{aligned} l_w &= 2\pi N_\beta \cdot \sum_{j=1}^{N_\alpha} \{r_c + (2j-1)\, r_w\} \\ &= 2\pi N_\beta N_\alpha \cdot \frac{(r_c + r_w) + \{r_c + (2N_\alpha - 1)\, r_w\}}{2} \\ &= \frac{\pi L_\alpha L_\beta}{2r_w^2}\left(r_c + \frac{1}{2}L_\alpha\right) \quad (6) \end{aligned}$$

$$A_w = \pi r_w^2 \quad (7)$$

where r_c is the radius of the magnetic core. The resistance of the excitation coil can be written as,

$$R_w = \frac{l_w}{A_w} \cdot \rho = \frac{L_\alpha L_\beta \rho}{2r_w^4}\left(r_c + \frac{1}{2}L_\alpha\right) \quad (8)$$

When the above results are brought into (5), the reluctance of the magnetic core is obtained as follows:

$$R_{mw} = \frac{1.11 \times f \cdot L_\beta \{(L_\alpha + r_c) - r_c\}}{\rho \{(L_\alpha + r_c) + r_c\}} \quad (9)$$

Because the permeability of both magnetic core and magnetic yoke materials are fairly high, their reluctance are much smaller than that of air medium. In order to ensure the detection effect and stability, it is necessary to increase the reluctance of the magnetic core to a certain extent to ensure that the magnetic flux density of the detection environment meets the detection requirements. Equation (9) shows that in order to achieve this goal, the winding width of excitation coils should be increased and the magnetic core radius should be reduced.

Because of the limitation of workpiece size on winding width of excitation coils, combined with the conventional workpiece size, we set the winding width L_β is 10 mm. In order to determine the radius of magnetic cores, finite element simulation experiments were carried out on cores with different cross-sectional areas in magnetic fields with the same power consumption to explore the relationship between the magnetic flux density at the core and the radius of the magnetic core, as shown in Fig. 3.

As shown in Fig. 3, the magnetic flux density decreases slowly with the increase of core radius. When the core radius increases to 3 mm, the magnetic field reaches saturation. The

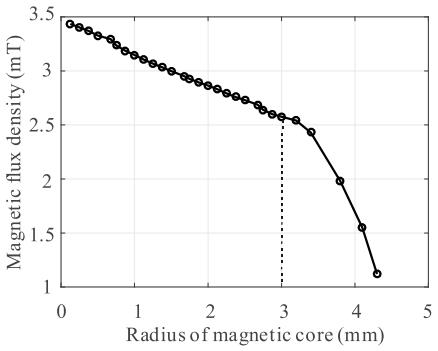

FIGURE 3. The relationship between magnetic core radius and magnetic flux density.

influence of edge effect on magnetic flux density is far greater than that of core itself, which leads to a significant decrease in magnetic flux density. Therefore, $r_c = 3$ mm is the best choice for detection and the highest stability.

The equivalent permeability theory is used to simplify other reluctances except magnetic core in (1). $\mu_1 \gg 1$, $\mu_4 \gg 1$, and $\mu_{\gamma 2} \gg 1$. The order of magnitude in these three is 10^3, so they are approximated to μ_r [15]. Because the material used in the magnetic core is similar to the magnetic yoke and is closely connected, the magnetic core is regarded as the magnetic yoke, which has no influence on the analysis results. The simplified reluctance is as follows:

$$\begin{aligned} R_m &= \frac{1}{\mu_0}\sum_{k=1}^{m-1}\frac{l_k}{\mu_e A_k} \\ &= \frac{1}{\mu_0\mu_r}\left(\frac{l_1}{nA}+\frac{l_{\gamma 2}}{A}+\frac{l_4}{A}\right)+\frac{1}{\mu_0}\left(\frac{l_2}{nA}+\frac{l_3}{A}+\frac{l_{\gamma 1}}{A}\right) \\ &= \frac{1}{\mu_0\mu_r A}\left(l-l_2-l_3-l_{\gamma 1}\right)+\frac{1}{\mu_0 A}\left(l_2+l_3+l_{\gamma 1}\right) \\ &\quad +\frac{1-n}{n}\frac{l_1}{\mu_0\mu_r A}+\frac{1-n}{n}\frac{l_2}{\mu_0 A} \\ &= \frac{1}{\mu_0 A}\frac{l+\left(l_2+l_3+l_{\gamma 1}\right)\left(\mu_r-1\right)}{\mu_r}+\sigma_1+\sigma_2, \\ &\quad n\geq 1, \quad n\in R \end{aligned} \tag{10}$$

$$\sigma_1 = \frac{1-n}{n}\frac{l_2}{\mu_0 A} \tag{11}$$

$$\sigma_2 = \frac{1-n}{n}\frac{l_1}{\mu_0\mu_r A} \tag{12}$$

where m, l, and μ_e, are the terms number of a polynomial in (2), equivalent magnetic circuit length and equivalent relative permeability, respectively. Let A, and nA be the equivalent cross-sectional area of magnetic circuit with the workpiece and the equivalent cross-sectional area of the magnetic yoke, where $n \geq 1, n \in R$, $\frac{1-n}{n} \in (-1, 0]$. As a non-detection area, coupling airgaps 1 are far away from the measured weld bead. It is conditional to reduce the reluctance by increasing the coupling area. The effect of σ_1 on total reluctance can be neglected when n is increased. The influence of the magnetic yoke on the total reluctance also depends on the cross-sectional area. When $n = 1$, $\sigma_2 = 0$, magnetic yokes have no effect on the total reluctance. When $n > 1$, $\sigma_2 < 0$, magnetic yokes will reduce the effect on the total reluctance. In summary, the influence of coupling airgap far from the measured weld beads and magnetic yokes on the reluctance change can be controlled artificially, which is a controllable change factor. This paper does not study them in depth. Because $\mu_r \gg 1$, (10) can be simplified as,

$$\begin{aligned} R_m &= \frac{1}{\mu_0 A}\left(\frac{l}{\mu_r}+l_2+l_3+l_{\gamma 1}\right)+\sigma_1+\sigma_2 \\ &= \frac{1}{\mu_0}\left(\frac{l_2}{A_2}+\frac{l_3}{A_3}+\frac{l_{\gamma 1}}{A_{\gamma 1}}\right)+\eta' \end{aligned} \tag{13}$$

where $\eta' \ll 1$. A_2 can be increased by increasing the cross-sectional area of the magnetic yoke. So the influence of R_2 on the total reluctance can be neglected under the condition of satisfying a certain cross-sectional area. Therefore, the mathematical model of the detection system including the main factors affecting the change of reluctance is as follows:

$$R_m = \frac{1}{\mu_0}\left(\frac{l_3}{A_3}+\frac{l_{\gamma 1}}{A_{\gamma 1}}+\eta\right), \quad \eta = \frac{l+\frac{1-n}{n}l_1}{\mu_r A}+\frac{l_2}{A_2} \tag{14}$$

where η is the fluctuation factor, $\eta \ll 1$. It is affected by the cross-sectional area of the magnetic yoke and the coupling area of coupling airgaps 1. As can be seen from the above equation, the difference of small size welding quality leads to the change of physical characteristics in the magnetic circuit [16], [17], and then changes the reluctance. Therefore, the non-destructive testing of small size welds can be achieved by measuring the reluctance.

Because the reluctance characteristics are stable and accurate, the model has significant advantages in the detection of small size weld bead. The reluctance change of closed magnetic circuit mainly depends on the physical properties of the weld defects and the coupling airgaps 2 which is close to the weld. However, due to the close distance between the two and the similar length and volume of the air medium, the coupling error produced by coupling airgaps 2 has the same ability of change to the reluctance with the weld defects. An optimization method is needed to attenuate the coupling error, which will be studied in detail in this paper.

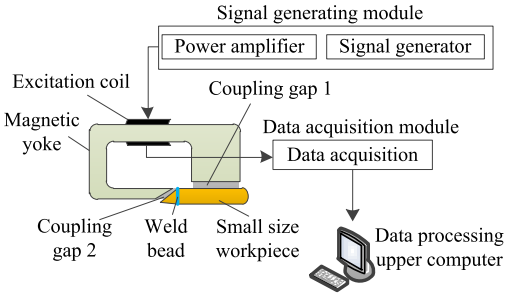

FIGURE 4. The structural diagram of the detection system.

B. APPLICATION OF THE MODEL

Non-destructive testing models for small size weld bead have been established. The main factors affecting the reluctance in a closed magnetic circuit are the weld defect and the coupling airgap close to the weld bead. Since the distance between coupling airgaps 2 and the weld defect are small, the reluctance cannot be reduced by increasing the coupling area, which brings about difficulty in the detection work.

In order to further study the non-destructive testing method based on reluctance measurement, a non-destructive testing system for small size weld bead was established according to the testing model. The detection system is composed of a signal generating module, detection module, data acquisition module and data processing upper computer. Its structural diagram is shown in Fig. 4.

In Fig. 4, the signal generating module is mainly composed of a signal generator and a power amplifier. After the signal is generated, the power is amplified. And the alternating magnetic field is generated by the excitation coil to magnetize the

workpiece and the weld bead. The detection module consists of excitation coils, magnetic cores, magnetic yokes, measured workpieces and coupling airgaps. Under the affect of alternating magnetic field, the qualified weld and the defective weld will show different reluctance characteristics. Data acquisition module collects relevant characteristic data. The data is sent to the data processing upper computer for analysis to obtain coupling error and reluctance change information. The upper computer recognizes and reduces the coupling error by software algorithm, which weakens the influence. And it classifies the reluctance information to realize the inspection of small size welding quality.

III. REALIZATION OF REDUCING COUPLING ERROR

A. COST-SENSITIVE SUPPORT VECTOR MACHINE

Aiming at the problem that the detection system can not distinguish the effect of weld defects and coupling airgaps on reluctance change, we construct cost-sensitive support vector machine (CS-SVM) to solve it. Through a large number of coupling experiments, we obtained the relevant feature data and trained them. It enables the detection system to distinguish weld defects and coupling airgaps, and assists the reluctance measurement method to achieve small size weld defects detection.

In practical fault diagnosis, on the one hand, the number of qualified welded workpiece samples on the production line is far more than that of defective samples, which leads to the imbalance of sample set data. Qualified sample data is obviously more than defective sample data. The basic support vector machine (SVM) has good classification performance for class-balanced sample set, but poor classification performance for class-unbalanced sample set [18]. On the other hand, it is much more harmful to classify the fault types into normal ones than to classify the normal types into fault ones. The basic SVM considers that the cost of classifying the normal samples into the fault ones is the same as that of classifying the fault samples into the normal ones. Therefore, the basic SVM will produce over-fitting in class-unbalanced samples, ignoring classes with fewer samples [19]. CS-SVM gives different classification costs to different samples. This method is more suitable for detection of small size weld defects in this paper.

Let the class-unbalanced sample set be $\{(x_i, y_i)\}_{i=1}^{k}$, where x_i, y_i, and k are the ith sample in sample set, label of the ith sample and number of samples, respectively. The known support vectors are $\omega \cdot x_i + b = -1, y_i = -1$ and $\omega \cdot x_i + b = 1, y_i = +1$, where ω and b are the normal vector of the hyperplane and the constant term. SVM maximizes the distance between support vectors by constructing hyperplane as a decision surface [20]. Since most of the practical problems are non-linear, it is necessary to map the sample points to the high-dimensional space Z, that is $x \to \varphi(x)$. Support vector is then changed to,

$$\begin{cases} \omega \cdot \{\varphi(x)\} + b = 1 - \xi_i \\ \omega \cdot \{\varphi(x)\} + b = -1 + \xi_i \end{cases} \tag{15}$$

where ξ_i is the slackness, $\xi_i \geq 0$. The distance between support vectors is as follows:

$$D = \frac{\omega}{\|\omega\|} \cdot \{\varphi(x_1) - \varphi(x_2)\} = \frac{2}{\|\omega\|} \tag{16}$$

After analysis, the main factors affecting detection of weld defects include the coupling airgap l_3, magnetic induction intensity B of magnetic circuit and inductance L of excitation coils. And there is a non-linear relationship between L and R_m. They are stable in a closed magnetic circuit and easy to be measured. So we select the above three groups of attributes as features. CS-SVM adds misclassification cost parameters C_1 and C_2 on the basic SVM. When different samples are misclassified, they will be given different misclassification costs. The original problem of CS-SVM is as follows:

$$\begin{aligned} &\max D = \min \frac{1}{2}\omega^T\omega + C_1 \sum_{i \in I_1} \xi_i + C_2 \sum_{i \in I_2} \xi_i \\ &s.t. \begin{cases} y_i \left(\omega^T \cdot \varphi(x_i) + b\right) \geq 1 - \xi_i \\ \xi_i \geq 0, \quad i = 1, 2, \cdots, k \end{cases} \end{aligned} \tag{17}$$

where $I_1 = \{i | y_i = +1\}$ and $I_2 = \{i | y_i = -1\}$. We usually use the inverse proportion of two type samples number as the ratio of the misclassification cost parameters [21]. We use Lagrange multiplier method and establish Lagrange function. The reverse problem of the original problem can be obtained by finding partial derivatives of ω and b, and making them equal to zero [22]. The antithetical problem can be written as,

$$\begin{aligned} &\max \chi(\alpha) = \sum_{i=1}^{k} \alpha_i - \frac{1}{2} \sum_{i=1}^{k} \sum_{j=1}^{k} \alpha_i \alpha_j y_i y_j \varphi(x_i)^T \cdot \varphi\left(x_j\right) \\ &s.t. \begin{cases} \sum_{i=1}^{k} \alpha_i y_i = 0 \\ 0 \leq \alpha_i \leq C_1, \quad i \in I_1 \\ 0 \leq \alpha_i \leq C_2, \quad i \in I_2 \end{cases} \end{aligned} \tag{18}$$

where $\{\alpha_i\}_{i=1}^{n}$ is the Lagrange multiplier and $\varphi(x_i)^T \cdot \varphi\left(x_j\right)$ can also be expressed as $k\left(x_i, x_j\right)$. The $k\left(x_i, x_j\right)$ is a kernel function, which is used to solve the interior product of $\varphi(x_i)$ and $\varphi\left(x_j\right)$ in high dimensional space.

B. OPTIMAL SELECTION OF PARAMETERS BY PSO

Due to the use of CS-SVM for assistant detection, misclassification cost parameters C_1, C_2 and kernel width λ has a great impact on the performance of CS-SVM. We need to adopt an algorithm to calculate the optimal values of three parameters iteratively.

Particle swarm optimization algorithm (PSO) has a fast convergence speed and is less affected by the change of dimension. Therefore, we use PSO to iteratively update our position by tracking the optimal position of fitness in the position experienced by the individual and the optimal position of fitness searched by all the particles in the population, that is the individual extremums $P_{z,i,d}^{k}$ and the group

TABLE 1. The relevant parameter information of carbide saw blade.

Parameter	Value (mm)
External diameter	184
Internal diameter	16
Base thickness	1.5
Cutter teeth thickness	3
Weld bead width	0.5
Distance between coupling surface and weld bead	3.6

extremums $P^k_{g,i,d}$ [23]. Among them, the velocity of the ith particle in the d dimensional space is updated iteratively as follows:

$$V^{k+1}_{i,d} = \omega V^k_{i,d} + c_1 r_1 \left(P^k_{z,i,d} - X^k_{i,d}\right) + c_2 r_2 \left(P^k_{g,i,d} - X^k_{i,d}\right) \tag{19}$$

where V^k, V^{k+1}, X^k, and ω are the current velocity, the velocity of next iteration, current position and inertial weight, respectively. Larger inertia weight is beneficial to jump out of the local minimum, so as to facilitate global search. c_1 and c_2 are the coefficients, r_1, r_2 are the random numbers which range from 0 to 1. The position of particles is updated iteratively as followsčž

$$X^{k+1}_{i,d} = X^k_{i,d} + V^{k+1}_{i,d} \tag{20}$$

where $X^{k+1}_{i,d}$ is the position of next iteration.

We update the velocity and displacement of particles by using (19) and (20). We compare all individual and group extremums of each particle and update them until the maximum number of iterations or preset accuracy is achieved. Then stop the iteration update. Output misclassification cost parameters and kernel width when terminating iteration.

IV. SIMULATION MODELING

In order to verify the feasibility of the reluctance measurement method, we selected the carbide saw blade in Ø184 × 3/1.5 × 16 × 36T as the test sample to carry out the feasibility experiment. In a closed magnetic circuit, the magnetized part of the sample includes the saw blade base, the cutter teeth and the weld bead between them. The relevant parameter information of the sample is shown in Table 1.

In Table 1, the size of the weld bead between the saw blade base and the cutter teeth is minuscule. And the weld width is about 0.5 mm. The width of the weld bead is similar to that of the coupling airgap, and the distance between the weld bead and the coupling airgap is extremely small. As shown in Equation (15), the coupling error forms a strong interference on the detection of weld quality. Many factors make it difficult to detect the weld bead of the similar workpiece. The detection method based on reluctance measurement can solve the weld bead detection for this kind of workpiece. The carbide saw blades with cracks and cavities in the weld bead are enumerated, as shown in Fig. 5. Among them, the position marked by the red circle left is the defective weld bead where

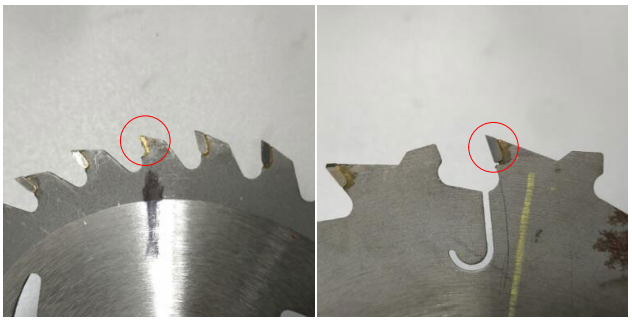

FIGURE 5. Carbide saw blades with weld cracks and cavities.

the cavities. And the position marked by the red circle right is the weld cracks.

ANSYS Maxwell finite element simulation software is used to build the model of weld bead qualify and defect according to the material, thickness, number of cutter teeth and defect type of the carbide saw blade. Then the simulation experiment is carried out. The simulation model consists of excitation coils (including signal generator), magnetic cores, magnetic yokes, carbide saw blade base, cutter teeth, weld beads and unsaturated alternating magnetic field. Label $y = +1$ is set to indicate qualified saw blade samples. Label $y = -1$ is set to indicate weld defect saw blade samples. The representative simulation model of carbide saw blades with qualified welds, weld defects and coupling airgaps is shown in Fig. 6.

In Fig. 6, we increase the cross-sectional area of the magnetic yoke coupled with the saw blade base. The purpose is to reduce the effect of coupling airgap on the total reluctance by increasing the coupling area. In order to prevent magnetic saturation, the cross-sectional area of the magnetic yoke should be obviously larger than that of the magnetic core. In Fig. 6 (b), the solder filling at the weld bead is insufficient, which is a lack of fusion defect. In Fig. 6 (c), there is an obvious coupling airgap between cutter teeth and magnetic yokes, and the airgap width is about 0.4 mm.

Common weld defects of carbide saw blades include cracks, pores, lack of fusion, cavities, etc [24]. In order to meet diversity of weld pattern in practical engineering, we adjust the volume and length of weld defects in simulation software numerous times to achieve comprehensive multiple values. The criteria for determining welding defects are shown in Table 2. This design method makes the welding defect samples sufficiently, and ensures the consistency of the finite element simulation results and the actual test results to the greatest extent.

While diversifying the values of welding defects, we randomly selected the value of coupling airgaps within 2 mm to simulate the coupling error in the experimental environment.

Through the finite element simulation experiment, the detection system has the highest sensitivity and the best effect to detect the weld defects of carbide saw blades when $\dot{I} = 20$ mA and $f = 300$ Hz. We also determined the relevant adaptive parameters of the simulation software by

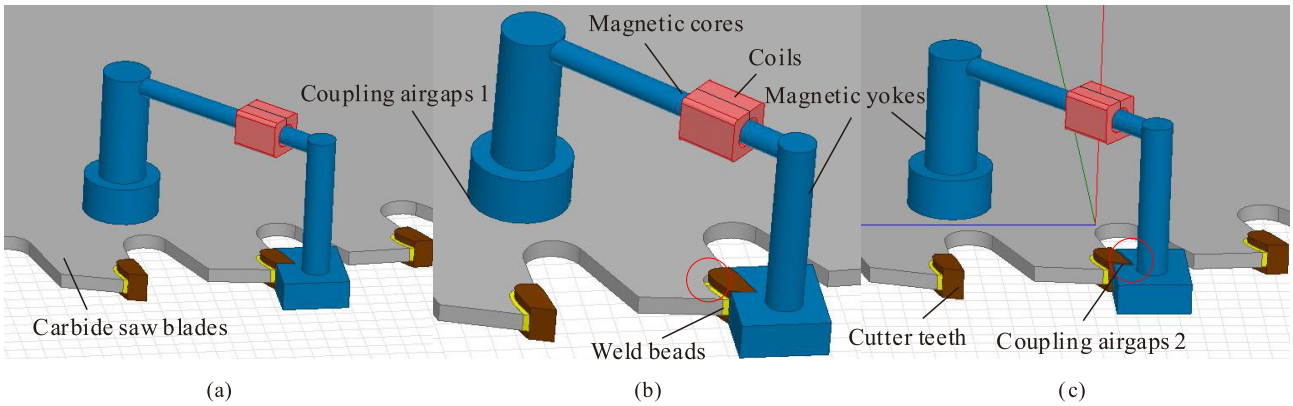

FIGURE 6. Simulation design diagram of detection system. (a) Qualified carbide saw blade. (b) Weld defect carbide saw blade. (c) Carbide saw blades with coupling airgaps.

TABLE 2. The criteria for determining welding defects.

Defect type	Defect volume (mm^3)	Defect length (mm)	Visibility
Cracks	0.03-0.24	1.1-5.4	Visible or invisible
Pores	0.1-1.2	0.5-1.3	Invisible
Lack of fusion	0.8-2.1	0.4-3.9	Invisible
Cavities	2.72-3.26	4.5-5.1	Visible or invisible

simulation experiment. The maximum iterations to characterize the stopping conditions of operations is 10, and the convergence error is 2%. When convergence error is not satisfied, the proportion of iterated encryption is 30%. The solution domain representing the solution range of the model is 5% in all directions outside the model.

V. EXPERIMENTAL TEST

According to the adaptive parameters, we test the reluctance measurement model by finite element simulation. The cutter teeth of the carbide saw blade is inspected one by one, so the mesh of the current inspecting weld bead is denser, while the mesh of the other welds is sparse. This method avoids the over-expenditure of 3D model on computer resources, effectively shortens the computing time, and provides a guarantee for large amount of data acquisition.

We collected and analyzed the three feature attributes of the excitation coil inductance L, the magnetic induction intensity B, and the coupling airgap l_3. The magnetic induction intensity was sampled once at intervals of 0.2 mm in the finite element simulation software. We obtained the magnetic induction intensity at sampling points with different coupling airgaps as shown in Fig. 7.

In Fig. 7, the peak variation of magnetic induction intensity was consistent under four different coupling airgaps. The peak value of cavities was the largest. The peak value of lack of fusion is larger. However, compared with the cavities, the peak value decreases greatly. The peak value of pores and cracks is smaller, and the peak value of pores is slightly larger than that of cracks. The peak value of qualified welding is the smallest. We refine the sampling interval of the sampling points where the peak of magnetic induction intensity is located in Fig. 7 to determine the peak value and the exact sampling points where the peak occurs, as shown in Table 3.

In Table 3, with the increasing of coupling airgaps, the peak magnetic induction intensity at sampling points of various weld defect types decreases gradually. Under the same coupling airgap, the peak values of magnetic induction intensity corresponding to cracks, pores, lack of fusion and cavities increase in proper order. The sampling points with peak have the distribution regularity. The sampling points where the peak of the same defect type are distributed in the same region. The results show that there is a correlation between the magnetic induction intensity and the coupling airgap in the magnetic circuit, which shows a certain objective law and is suitable for data analysis as feature attributes.

We test the above simulation models by adjusting the parameters one by one, and select two representative groups of results to compare, as shown in Fig. 8.

In Fig. 8, it is shown that the magnetic induction intensity in a closed magnetic circuit is greater than that around the magnetic circuit, and the maximum amplitude of the magnetic induction intensity is found at the detected cutter teeth. The white circle in Fig. 8 is the weld bead under test. In Fig. 8 (a), the magnetic induction intensity at the weld bead is uniform, which indicates the qualified weld bead will not interfere with the magnetic flux. In Fig. 8 (b), the amplitude of magnetic induction intensity at weld bead fluctuates seriously, ranging from 0.5 T to 3 T. It shows that weld defects have great interference on flux path, and also change physical properties such as reluctance.

Reluctance and inductance of excitation coil have different results under different coupling airgaps. We use finite element simulation software to quantitatively explore the reluctance and inductance corresponding to weld defects with different volumes of carbide saw blades under ideal coupling conditions, as shown in Table 4.

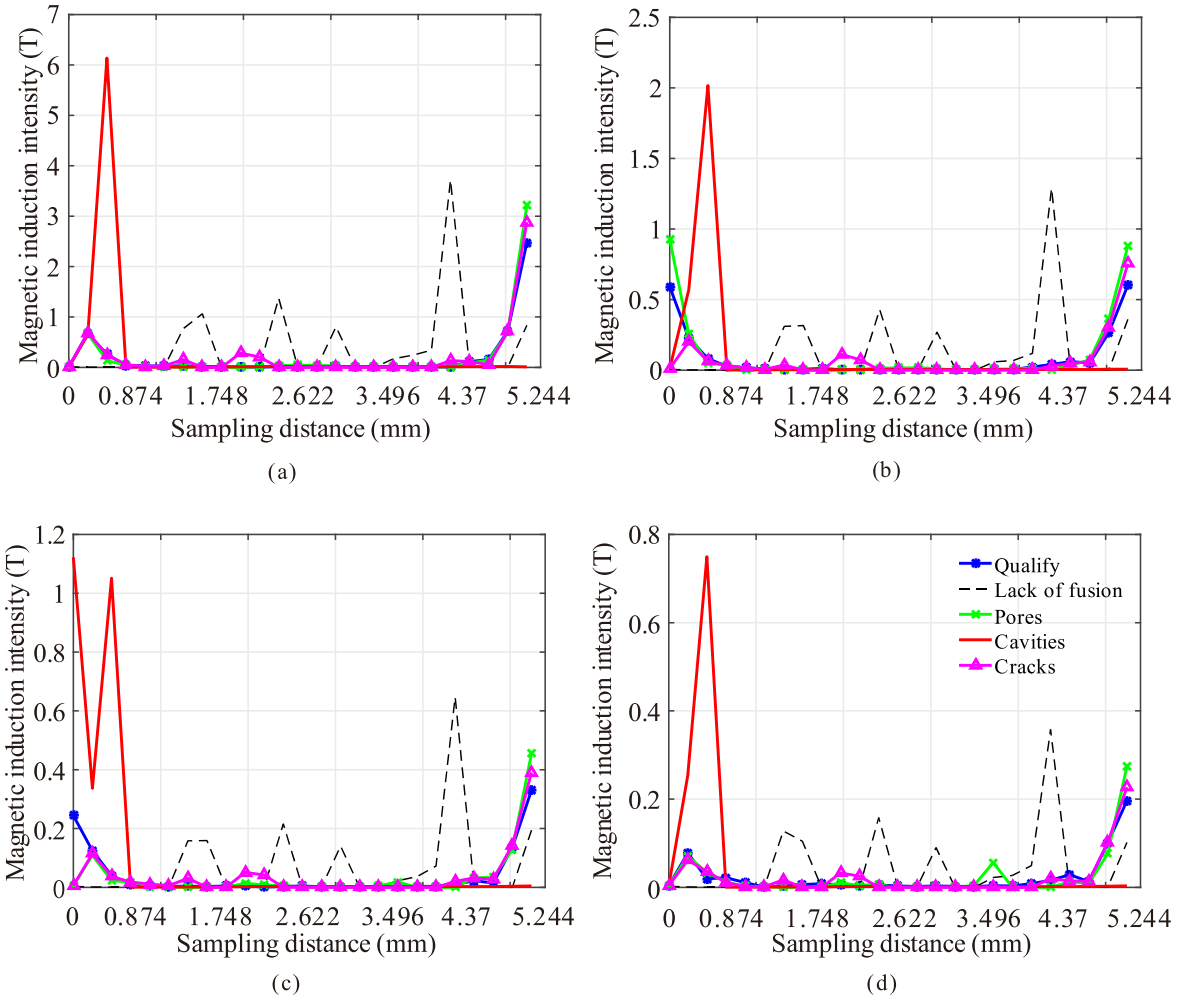

FIGURE 7. Magnetic induction intensity at sampling points with different coupling airgaps. (a) The coupling airgap is 0.01 mm. (b) The coupling airgap is 0.4 mm. (c) The coupling airgap is 1 mm. (d) The coupling airgap is 1.5 mm.

TABLE 3. Peak contrast of magnetic induction intensity.

Coupling airgaps (mm)	Cracks		Pores		Lack of fusion		Cavities		Qualified weld	
	Peak value (T)	Sampling point (mm)	Peak value (T)	Sampling point (mm)	Peak value (T)	Sampling point (mm)	Peak value (T)	Sampling point (mm)	Peak value (T)	Sampling point (mm)
0.01	2.882	5.26	3.216	5.24	3.719	4.37	6.137	0.44	2.476	5.25
0.2	1.860	5.29	2.538	5.27	2.901	4.35	4.752	0.40	1.783	5.24
0.4	0.754	5.25	0.882	5.23	1.289	4.36	2.017	0.44	0.603	5.25
1	0.391	5.27	0.455	5.25	0.647	4.37	1.122	0.41	0.330	5.21
1.5	0.227	5.26	0.275	5.26	0.358	4.37	0.750	0.43	0.196	5.23

In Table 4, the reluctance of qualified weld bead is the smallest, and the inductance of excitation coil is the largest. The reluctance corresponding to cracks and pores increases slightly and the inductance decreases slightly. Lack of fusion corresponds to larger reluctance and smaller inductance. The maximum reluctance and the minimum inductance correspond to the cavities. The results show that different weld defects directly lead to the change of reluctance and coil inductance in a closed magnetic circuit. The larger the defect volume, the larger reluctance, the smaller the inductance and vice versa. The simulation results are consistent with the theoretical demonstration.

According to the relevant parameters of finite element simulation, we establish a detection system to carry out physical experiments. Among them, excitation coils are composed of copper enameled wire with a diameter of 0.11 mm, which are tightly wound on magnetic yokes, and the number of winding turns are 1000. We selected diverse groups of carbide saw blades with different defect types for experimental testing. Then we measured and recorded the coupling

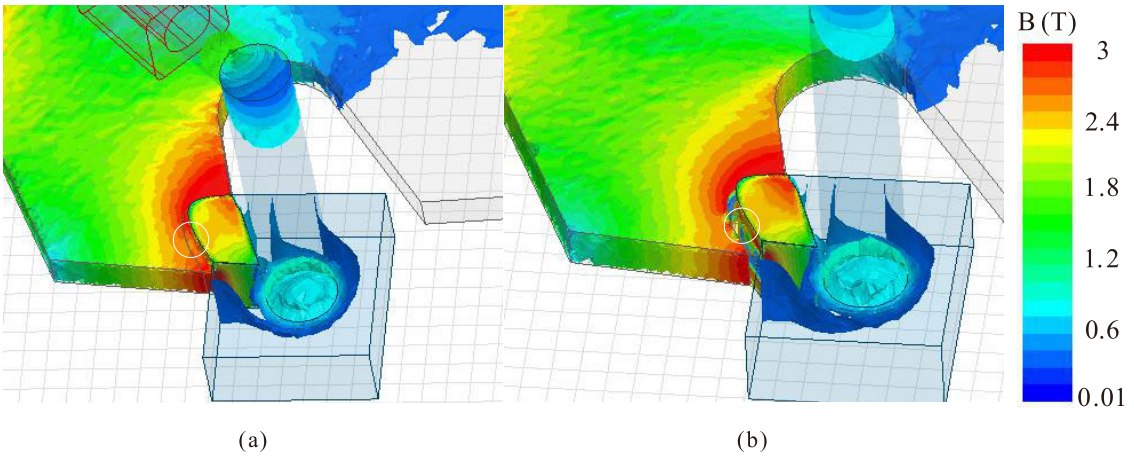

FIGURE 8. Distribution of magnetic induction intensity with qualified and defective weld bead carbide saw blades. (a) Qualified carbide saw blade. (b) Carbide saw blades with pores in weld bead.

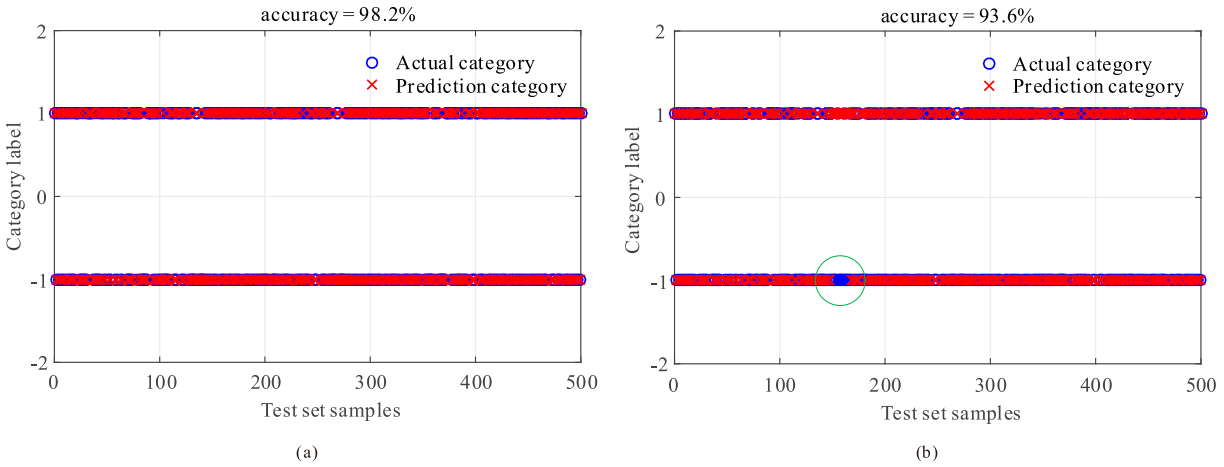

FIGURE 9. Comparison of classification results with two vector machines. (a) The improved CS-SVM. (b) The basic SVM.

TABLE 4. The reluctance and inductance corresponding to weld defects with different volumes.

Defect type	Defect volume (mm^3)	L (mH)	R_m (H^{-1})
Cracks	0.20	260.923	3.833×10^6
Cracks	0.09	261.107	3.830×10^6
Pores	0.54	260.084	3.845×10^6
Pores	0.32	260.349	3.841×10^6
Lack of fusion	1.35	252.431	3.961×10^6
Lack of fusion	1.78	251.745	3.972×10^6
Lack of fusion	0.97	253.056	3.952×10^6
Cavities	2.81	231.386	4.322×10^6
⋮	⋮	⋮	⋮
Qualified weld	/	261.872	3.819×10^6
Qualified weld	/	263.115	3.801×10^6

airgap l_3, the inductance L of excitation coils and the magnetic induction intensity B respectively by controlling the random value of the coupling airgap within 2 mm. The experiment collected 5000 sets data and randomly divided the training set and the test set according to the 9:1 ratio. In the training set, there were 2546 group qualified weld bead samples and 1954 group defective weld bead samples, which were formed by four kinds of weld defects. The proportion of qualified and defective data sets in test set is similar to training set. So the proportion of misclassification cost parameters is $C_1 : C_2 = 1 : 1.303$.

Applying the improved CS-SVM and the basic SVM to test 500 sets of data, we get the classification results with two kinds of vector machines for test sets as shown in Figure 9.

In Fig. 9, for identical test data sets, the classification errors of the basic SVM are significantly more than improved CS-SVM. According to statistics, the improved CS-SVM has only 9 wrong classification samples, and the classification accuracy rate is 98.2%. All the wrong classification samples were judged as defective saw blades by qualified weld saw blades. The basic SVM has 32 wrong classification samples, and the classification accuracy is 93.6%. There are mutual misjudgments between qualified weld

TABLE 5. Classification results of the improved CS-SVM.

Number	Defect types	l_3 (mm)	B (T)	L (mH)	Classification result	Actual result	Correct or not
1	Cracks	0.32	0.082	133.812	-1	-1	Yes
2	Qualified weld	1.1	0.055	91.542	+1	+1	Yes
3	Cavities	0.25	0.173	142.339	-1	-1	Yes
4	Lack of fusion	1.6	0.044	80.132	-1	-1	Yes
5	Pores	0.08	0.179	212.564	-1	-1	Yes
6	Qualified weld	0.5	0.082	109.527	-1	+1	No
7	Cavities	0.01	0.592	210.421	-1	-1	Yes
8	Pores	0.5	0.123	121.962	-1	-1	Yes
⋮	⋮	⋮	⋮	⋮	⋮	⋮	⋮
495	Cracks	0.08	0.137	186.015	-1	-1	Yes
496	Lack of fusion	0.05	0.269	203.594	-1	-1	Yes
497	Qualified weld	0.42	0.051	116.248	+1	+1	Yes
498	Cavities	0.16	0.195	154.863	-1	-1	Yes
499	Pores	0.03	0.254	238.195	-1	-1	Yes
500	Lack of fusion	0.14	0.154	169.955	-1	-1	Yes

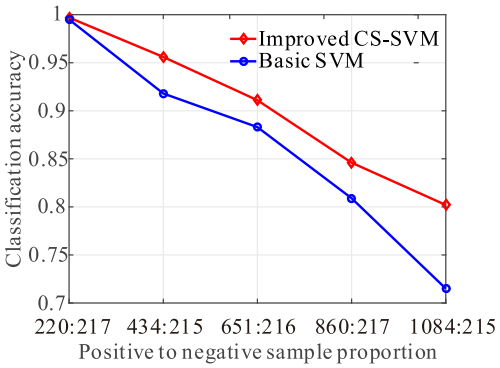

FIGURE 10. Classification results of different methods for different proportion sample sets.

samples and defective saw blade samples. The circle in Figure 9 (b) is the sample set of the defective saw blade judged by the basic SVM as qualified. This kind of misclassification is unusually harmful, and results in serious consequences in engineering application. Therefore, the method based on reluctance measurement has excellent performance and reasonable model construction process, which is suitable for weld bead detection of large quantities workpieces on the production line. Relevant data for improved CS-SVM classification are shown in Table 5.

Through the exploration and verification after the experiment, we found that the nine groups of incorrect classification samples is that the thermal burns occurred in the weld bead due to high temperature welding, which affected the feature attribute data and led to the incorrect classification of individual samples. In later research, thermal burns will be included in the testing scope to make the detection method more effective.

Keeping the misclassification cost parameter in $C_1 : C_2 = 1 : 1.303$ unchanged, we then used five different sample sets with positive-negative sample ratio of 1:1, 2:1, 3:1, 4:1, 5:1 to test and compare the classification performance of the improved CS-SVM and the basic SVM. The results are shown in Fig. 10.

In Fig. 10, the improved CS-SVM effectively improves the diagnostic accuracy of defect samples compared with the basic SVM. In the process of increasing sample proportion, the distinction between the two methods becomes increasingly obvious. The improved CS-SVM is less affected by sample imbalance performance and has strong generalization ability.

It is suitable for class-unbalanced samples and sample set data with different misclassification costs.

VI. CONCLUSION

As a new non-destructive testing method for small size weld bead, the reluctance measurement demonstrated in this study achieves high efficiency and accuracy, and can be used to detect a large number of workpieces on the production line. The new method establishes a closed magnetic circuit reluctance measurement model to explore the characteristics of small size weld defects, and obtains the quantitative relationship between closed magnetic circuit reluctance and weld defects. To investigate the coupling error caused by the coupling surface close to the weld bead, we use the improved CS-SVM to effectively reduce the error interference, and get the following conclusions:

1) Under the same coupling airgap, the peak values of magnetic induction intensity corresponding to cracks, pores, lack of fusion and cavities increase in proper sequence, and the ability to change reluctance also increases in proper sequence.
2) The improved CS-SVM can effectively reduce the interference of coupling airgaps of general workpiece on reluctance measurement, and provide a guarantee for non-destructive detection of small size weld bead.
3) A large number of simulation data verify that this new method is used to detect the weld bead of representative carbide saw blades, and the accuracy rate is 98.2%. The new method successfully solves the difficult problem of detecting small size weld defects in production line which can not be solved by traditional non-destructive testing method.

4) Compared with the basic SVM, the improved CS-SVM not only has excellent performance and high diagnostic accuracy in handling class-unbalanced samples, but also strictly avoids the possibility that defective weld samples are misclassified into qualified ones, which provides a guarantee for safe production.

REFERENCES

[1] E. G. Tarpara and V. H. Patankar, "Real time implementation of empirical mode decomposition algorithm for ultrasonic nondestructive testing applications," *Rev. Sci. Instrum.*, vol. 89, no. 12, pp. 1–2, Dec. 2018, doi: 10.1063/1.5074152.

[2] A. Mirala and S. R. Sarraf, "Detection of surface cracks in metals using time-domain microwave non-destructive testing technique," *IET Microw., Antennas Propag.*, vol. 11, no. 4, pp. 564–565, Apr. 2017, doi: 10.1049/iet-map.2016.0587.

[3] H. Miyazaki, Y. Nomura, H. Sugai, M. Iijima, S. Inasawa, and H. Kamiya, "Liquid penetration as a simple detection method for structural differences in particulate films prepared from slurries," *Powder Technol.*, vol. 303, pp. 60–61, Dec. 2016, doi: 10.1016/j.powtec.2016.09.011.

[4] M. Dissanayake, D. Carswell, M. Corsar, T. P. Sattar, M. Sutcliffe, P. S. Lowe, and T.-H. Gan, "Automated application of full matrix capture to assess the structural integrity of mooring chains," *IEEE Access*, vol. 6, pp. 75560–75561, Nov. 2018, doi: 10.1109/ACCESS.2018.2883378.

[5] P. Rodríguez-Gonzálvez and M. Rodríguez-Martín, "Weld bead detection based on 3D geometric features and machine learning approaches," *IEEE Access*, vol. 7, pp. 14714–14727, 2019, doi: 10.1109/ACCESS.2019.2891367.

[6] T. Gurieva, E. Marushin, A. Mednikov, I. Rodin, and I. Sokolov, "NDT status of PF1 coil welds," *IEEE Trans. Appl. Supercond.*, vol. 28, no. 4, pp. 1–5, Jun. 2018, doi: 10.1109/TASC.2018.2796629.

[7] D. Wu, L. Zhitian, W. Xiaohong, and S. Lingxin, "New NDT method for ferromagnetic materials based on differential permeability," *Chin. J. Sci. Instrum.*, vol. 38, no. 6, pp. 1490–1497, Jun. 2017.

[8] T. D. Carrigan, B. E. Forrest, H. N. Andem, K. Gui, L. Johnson, J. E. Hibbert, and R. Sloan, "Nondestructive testing of nonmetallic pipelines using microwave reflectometry on an in-line inspection robot," *IEEE Trans. Instrum. Meas.*, vol. 68, no. 2, pp. 586–594, Feb. 2019, doi: 10.1109/TIM.2018.2847780.

[9] J. Brizuela, J. Camacho, G. Cosarinsky, J. M. Iriarte, and J. F. Cruza, "Improving elevation resolution in phased-array inspections for NDT," *NDT & E Int.*, vol. 101, pp. 1–16, Sep. 2019, doi: 10.1016/j.ndteint.2018.09.002.

[10] C. Jain, *Principles of Electromagnetic Theory*. Oxford, U.K.: Alpha Science, 2017, pp. 211–213.

[11] U. F. Samedova and S. M. Hasanli, "Magnetoresistance in granular metal-dielectric composites," *Surf. Eng. Appl. Electrochem*, vol. 54, no. 2, pp. 132–133, May 2018, doi: 10.3103/S1068375518020114.

[12] X. Liu, Y. Yang, and J. Zhang, "Investigation on coupling effects between surface wear and dynamics in a spur gear system," *Tribol. Int.*, vol. 101, pp. 386–387, Sep. 2016, doi: 10.1016/j.triboint.2016.05.006.

[13] H. T. Liu, J. Schneider, A. Stöcker, A. Franke, F. Gao, H.-Y. Song, Z.-Y. Liu, R. Kawalla, and G.-D. Wang, "Microstructure and texture evolution in non-oriented electrical steels along novel strip casting route and conventional route," *Steel Res. Int.*, vol. 87, no. 5, p. 590, 2016, doi: 10.1002/srin.201500145.

[14] J. Nam, W. Lee, E. Jung, and G. Jang, "Magnetic navigation system utilizing a closed magnetic circuit to maximize magnetic field and a mapping method to precisely control magnetic field in real time," *IEEE Trans. Ind. Electron.*, vol. 65, no. 7, pp. 5675–5677, Jul. 2018, doi: 10.1109/TIE.2017.2782220.

[15] J. Wang, B. Zhou, X. Liu, W. Wu, L. Chen, B. Han, and J. Fang, "An improved target-field method for the design of uniform magnetic field coils in miniature atomic sensors," *IEEE Access*, vol. 7, pp. 74803–74814, Jun. 2019, doi: 10.1109/ACCESS.2019.2920955.

[16] W. Xu, C. Guo, S. Guo, and X. Li, "A novel quality defects diagnosis method for the manufacturing process of large equipment based on product gene theory," *Symmetry*, vol. 11, no. 5, p. 685, May 2019, doi: 10.3390/sym11050685.

[17] J. Abellán, C. J. Mantas, and J. G. Castellano, "A random forest approach using imprecise probabilities," *Knowl.-Based Syst.*, vol. 134, pp. 35–36, Jul. 2017, doi: 10.1016/j.knosys.2017.07.019.

[18] X. Lu, T. Hu, Y. Zhang, and B. Fan, "Robust clustered support vector machine with applications to modeling of practical processes," *IEEE Access*, vol. 6, pp. 75143–75154, Nov. 2018, doi: 10.1109/ACCESS.2018.2883433.

[19] D. He, J. Peng, J. Hu, T. Li, and W. Jia, "Bearing fault diagnosis based on a modied CS-SVM model optimized by an improved FOA algorithm," *J. Vib. Shock*, vol. 37, no. 18, pp. 109–110, Sep. 2018, doi: 10.13465/j.cnki.jvs.2018.18.015.

[20] M. Gaudioso, E. Gorgone, M. Labbé, and A. M. Rodríguez-Chía, "Lagrangian relaxation for SVM feature selection," *Comput. Oper. Res.*, vol. 87, pp. 141–142, Jun. 2017, doi: 10.1016/j.cor.2017.06.001.

[21] S. Wang, Y.-Y. Yuan, C.-Y. Zhu, D.-M. Kong, and Y.-T. Wang, "Discrimination of polycyclic aromatic hydrocarbons based on fluorescence spectrometry coupled with CS-SVM," *Measurement*, vol. 139, pp. 476–477, Jan. 2019, doi: 10.1016/j.measurement.2019.01.087.

[22] M. Bi, J. Yu, X. Miao, T. Huang, L. Li, H. Chi, and W. Hu, "A powerful equalizer based on modified SVM classifier without nonlinear kernel enabled 100-Gb/s NG-EPON system with 10-G class," *IEEE Accessx*, vol. 7, pp. 71188–71189, May 2019, doi: 10.1109/ACCESS.2019.2919344.

[23] C. Yeom and K. Kwak, "Incremental granular model improvement using particle swarm optimization," *Symmetry*, vol. 11, no. 3, p. 390, Mar. 2019, doi: 10.3390/sym11030390.

[24] R. L. Lemaster and J. Schultz, "The use of acousto-ultrasonics to determine the quality of the brazing of carbide-tipped cutting tools," *Wood Mater. Sci. Eng.*, vol. 11, no. 3, p. 166, 2016, doi: 10.1080/17480272.2016.1146798.

HONGMIN WANG received the Ph.D. degree. He is currently a Professor with the Department of Automation, Harbin University of Science and Technology. His research interests include electronic information and embedded detection technology.

MENG WANG is currently pursuing the master's degree with the Department of Automation, Harbin University of Science and Technology. His research interests include detection technology and intelligent systems.